Adsorbing CNCl on pristine, C-, and Al-doped boron nitride nanotubes
A density functional theory study

Doust Mohammadi, Mohsen; Abdullah, Hewa Y.; Biskos, George; Bhowmick, Somnath

DOI
10.1016/j.comptc.2022.113980

Publication date
2023

Document Version
Final published version

Published in
Computational and Theoretical Chemistry

Computational and Theoretical Chemistry 1220 (2023) 113980

Contents lists available at ScienceDirect

Computational and Theoretical Chemistry

journal homepage: www.elsevier.com/locate/comptc

Adsorbing CNCl on pristine, C-, and Al-doped boron nitride nanotubes: A density functional theory study

Mohsen Doust Mohammadi [a], Hewa Y. Abdullah [b,*], George Biskos [c,d], Somnath Bhowmick [c]

[a] School of Chemistry, College of Science, University of Tehran, Tehran 14176, Iran
[b] Physics Education Department, Faculty of Education, Tishk International University, Erbil 44001, Kurdistan Region, Iraq
[c] Climate and Atmosphere Research Centre, The Cyprus Institute, Nicosia 2121, Cyprus
[d] Faculty of Civil Engineering and Geosciences, Delft University of Technology, Delft 2628 CN, the Netherlands

ARTICLE INFO

Keywords:
Boron nitride nanotube
Cyanogen chloride, DFT
NBO
Wave function analysis

ABSTRACT

The density functional theory (DFT) framework was used to investigate the intermolecular interactions between cyanogen chloride (CNCl) pollutant gas molecule with pristine boron nitride nanotubes (BNNT), Al-doped boron nitride nanotubes (BNAlNT), and carbon boron nitride nanotubes (BC_2NNT). The geometric structures of the resulting systems have been optimized using different methods, including B3LYP-D3(GD3BJ)/6-311G(d), ωB97XD/6-311G(d), and M06-2X/6-311G(d). The computed adsorption energies suggest that the studied nanotubes can enhance adsorption of CNCl, and thus promote its detection when employed as sensing materials. Wave function analysis has been implemented to study the type of intermolecular interactions at ωB97XD/6-311G(d,p) level of theory. Natural bond orbital (NBO) analysis has been used to study the charge transfer and bond order. Quantum theory of atoms in molecules (QTAIM) analysis has also been used to determine the type of interactions between the target gas and the nanotubes. To investigate the weak intermolecular interactions we also carried out non-covalent interaction analysis (NCI). The results also indicate that the CNCl-nanotube systems are created through physisorption as they are dominated by non-covalent interactions. The predicted adsorption energies increase as follows: BNAlNT: −1.175 eV > BC_2NNT: −0.281 eV > BNNT: −0.256 eV; this shows that the aluminum-doped boron nitride nanotube is the best option from promoting adsorption of the target gas among them. The HOMO–LUMO energy gaps were as follows: BNNT: 7.090, BNAlNT: 9.193, and BC_2NNT: 7.027 eV at B3LYP-D3/6-311G(d) level of theory.

1. Introduction

To determine the properties of nanomaterials and consequently to investigate their appropriateness for specific applications we need to understand the intermolecular interactions with chemical species present in their immediate environment [1–5]. Nanotubes, nanosheets, and nanocages, are among the materials that have been explored in this respect for a wide number of applications. Using computational tools, and especially quantum computing and molecular dynamics of high accuracy [6], great efforts have been made to study the properties of these materials [7]. In addition, a number of studies have investigated the intermolecular interactions between such nanomaterials and highly reactive compounds, comprising one of the main motivations in the field of computational sciences [8–14].

Boron nitride nanotubes are among the different types of nanotubes that theoretically exhibit interesting properties including electrical and thermal conductivity, as well as mechanical stability [15]. To increase the reactivity of this type of nanotubes, changes in their structure can be made, e.g., by adding aluminum or gallium. This leads to the formation of a more polarized electron cloud, which in turn increases dramatically the reactivity of the nanotubes [16,17].

Shao et al. considered the effect of Al doping in the boron nitride nanotube for adsorbing CO_2 [18], whereas Mirzaei and his colleagues have studied in detail the role of aluminum in the structure of boron nitride nanotubes [19,20]. Another approach for enhancing their absorption capabilities is to add carbon to the structure of boron nitride nanotubes (i.e. BC_2NNT). Theoretical studies reported in the literature indicate that the use of these nanotubes can enhance physical and chemical adsorption of pollutant gases [21–23].

Cyanogen chloride (CNCl) is one of the most dangerous gases used in

* Corresponding author.
E-mail address: hewayaseen@gmail.com (H.Y. Abdullah).

https://doi.org/10.1016/j.comptc.2022.113980
Received 8 June 2022; Received in revised form 18 September 2022; Accepted 5 December 2022
Available online 10 December 2022

industry or produced as a by-product in organic synthesis. Exposure to CNCl can cause many symptoms including drowsiness, rhinorrhea, sore throat, etc. [24]. Developing sensors that can detect and measure the concentration of CNCl in the breathing air is therefore of particular importance for preventing exposure and minimizing associated risks at the workplace. To achieve that, a number of sensing approaches, including electrochemical [25], metal oxide semiconductor [26], graphene-based [27], and nanotube-based [28] sensors, can be used to measure the concentration of CNCl in ambient air. In almost all of these cases, elements that can enhance adsorption of the target gas are highly useful as they can increase the sensitivity and improve the selectivity of the resulting sensors. Towards this direction, adsorption of CNCl by carbon nanocages has been studied by Soltani et al [29]. Aluminum nitride nanotubes have also been investigated for this purpose by the same research group [30], whereas phosphorus-based nanomaterials have also been explored [31,32].

The main focus of this study is to investigate the adsorption of CNCl onto boron nitride, carbon boron nitride, and aluminum-doped boron nitride nanotubes using DFT framework. The rest of the paper is organised as follows. Section 2 provides all the details of our calculations and references to the relevant computational codes. The calculations for the geometry optimization and the identification of local minima are provided in Section 3.1, whereas the electronic structures are discussed in Section 3.2. The charge transfer and bond orders resulting from the natural bond orbital (NBO) analysis calculations are given in Section 3.3. Section 3.4, provides the quantum theory of atoms in molecules (QTAIM) analysis and discusses the type of intermolecular interactions. Finally, Section 4 summarizes the most important conclusions.

2. Computational details

Density functional theory is a framework that provides the study of many-body systems with a high number of atoms. In order to reduce the computational time while maintaining good accuracy, a basis set that best covers the integration space is selected. Benchmark studies have shown that the 6-311G(d) (i.e. split-valence triple-zeta) basis set well approximates the space required for the carbon, nitrogen, boron, and chlorine atoms [33–37]. A number of processes including dispersion is also considered for functional selection, whereas long- and short-range interactions are also taken into account due to their high importance. In this study, functionals ωB97XD [38], M06-2X [39,40], and B3LYP-D3 (GD3BJ) [41–43] are used to optimize the geometry of the resulting structures. Functional ωB97XD is employed to investigate the wave function analysis. The Gaussian 16 software was employed to perform SCF calculations [44]. All default settings and threshold limits are used, whereas no additional settings are applied in our calculations. Gauss-View 6.0.16 [45] is employed to build the system models. The NBO software version 3.1 [46–48] included in Gaussian is also used to carry out wave function analysis, whereas Multiwfn [49] was employed to interpret the results obtained from NBO and the QTAIM analysis.

The following formula was used to calculate the adsorption energy (E_{ads}) of each system:

$$E_{ads} = E_{tube/gas} - E_{tube} - E_{gas} + \Delta E_{BSSE} + \Delta E_{ZPE} \quad (1)$$

Here $E_{tube/gas}$ refers to the total energy of the gas/nanotube system, whereas E_{gas} and E_{tube} are the energies of the isolated target gas and the nanotubes, respectively. ΔE_{BSSE} and ΔE_{ZPE} are respectively the basis set superposition error and zero point energy corrections, which are calculated as follows [50–52]:

$$\Delta E_{BSSE} = E_{cluster} - E_{tube}^{cluster} - E_{gas}^{cluster}$$

$$\Delta E_{ZPE} = E_{cluster,ZPE} - E_{tube,ZPE} - E_{gas,ZPE} \quad (3)$$

Here $E_{cluster}$ denotes the energy of the cluster (target gas + nanotube), $E_{tube}^{cluster}$ is the energy of the nanotube in the cluster structure, and $E_{gas}^{cluster}$ is the calculated energy of the target gas in the cluster structure. $E_{tube,ZPE}$ and $E_{gas,ZPE}$ are total energy of isolated nanotube and gas containing zero point energy corrections, and are determined by the relaxed isolated structures through frequency calculations.

3. Result and discussion

3.1. Geometry optimization procedure

In the first step, both the CNCl structure and each of the boron nitride, carbon and aluminum-doped boron nitride nanotubes is optimized separately. Calculations for each of the structures are performed by method B3LYP-D3(GD3BJ)/6-311G(d), whereas the semi-emperical PM7 method was used to find a suitable first guess to provide input for the quantum chemistry calculations. That is, first all the isolated nanotubes are optimized by the PM7 method and then the optimized structure is introduced as input for DFT calculations to the Gaussian 16 software. The atomic equilibrium distances for the CNCl gas molecule are illustrated in Fig. 1.

The length (and diameter) of boron nitride single-wall armchair (5,5) nanotube has a 12.33-Å length. Including terminal hydrogens to the nanotubes in order to reduce boundary effects, the nanotube contains 110 atoms. Changing the morphology (e.g., using armchair- or zigzag-type nanotubes) or increasing the length or diameter of the nanotube does not affect the adsorption energy as indicated by previous studies [53–55]. When the size of the adsorbent and the nanotube are comparable, the results of the calculated adsorption energies are less valid. Therefore, the size of the nanotube must be much larger compared to the adsorbing species. Therefore, the choice of armchair (3,3) BNNT cannot be a suitable option. On the other hand, the choice of armchair (7,7) BNNT only increases the calculation time and will not have a significant effect on the calculated adsorption energies [8]. So, the reasonable choice is to use armchair (5,5) nanotubes boron nitride nanotube. Pristine boron nitride nanotube has been used to make BNAlNT. In this way, a boron atom is replaced by an Al atom and the whole structure is optimized again. Fig. 2 shows the nanotubes, where the bond lengths are changed slightly when the Al atom is replaced. This, in turn, affects the adsorption energy as we will discuss later.

The most challenging part of the molecular optimization process is finding the most stable gas and nanotube configuration. For this purpose, all possible states are investigated and the gas molecule placed at different distances from the outer surface of the nanotube to obtain the most stable adsorption energy. It should also be noted that in addition to changing the distance, the gas molecule is placed at different angles in order to choose the best option for the calculation of the adsorption energy from all possible configurations. Fortunately, nanotubes generally have a symmetrical geometric structure, which greatly simplifies the calculations. As shown in Fig. 3, there are only 4 distinct positions on the outer surface of the boron nitride nanotube that can qualify as adsorption sites (T_x).

First, the gas molecule is placed from its Cl head on top of the boron atom on the outer surface of the boron nitride nanotube having a vertical position. This is done for each of the other 3 mentioned adsorption sites. At the same time the gas molecule is rotated, and turned with the N head towards the nanotube. To find the optimum distance between the gas and the nanotube, we repeat the the calculations by changing the relative position between the gas and the nanotube with distance steps that

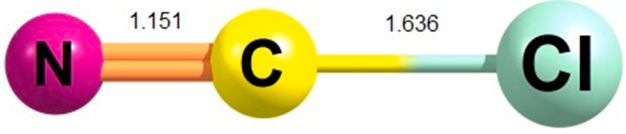

Fig. 1. Optimized CNCl molecule and associated bond lengths expressed in Ångstrom. The values are obtained by the ωB97XD/6-311G(d) model.

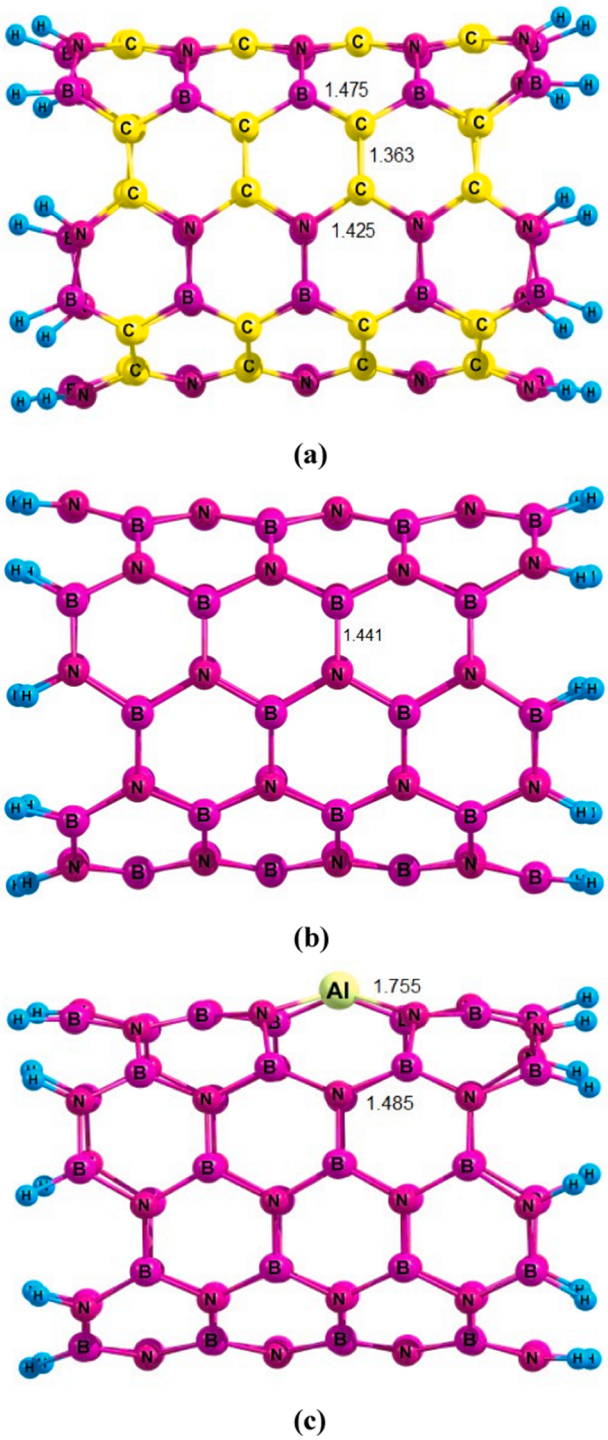

Fig. 2. Length of the equilibrium bonds between the constituent atoms of nanotubes **(a)** BC_2N, **(b)** BN, and **(c)** BNAl, obtained by the ωB97XD/6-311G(d) DFT method.

range from of 0.5 to 5 Å. In total, we generate 80 different geometric structures that are then introduced as input to the Gaussian software. We employ the PM7 method to save time and reduce computational cost, and a number of optimized configurations with this method are prepared for the next step. The criterion for selecting the best optimized geometries is the total molecular energy, which introduces the most stable configurations for DFT calculations.

Using this systematic method, the best optimized geometries are achieved(see Fig. 4). The method employed in this study was B3LYP-D3

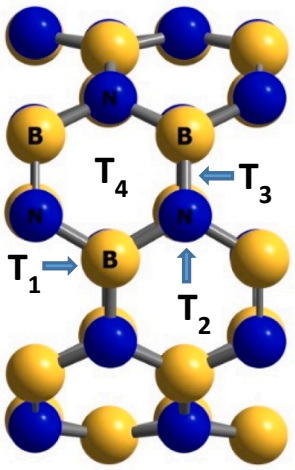

Fig. 3. Unit cells of the BNNT used for the DFT calculations. *Tx* positions are shown for the boron atom (*T*1), the nitrogen atom (*T*2), between the boron and the nitrogen atoms (*T*3), and for the hexagonal ring (*T*4).

(GD3BJ)/6-311G(d), but functionals M06-2X and ωB97XD were also used to compare the values of obtained adsorption energy (see Table 1). Each of these functionals, taking into account the shares of exchange and correlation energies, eventually leads to different amounts of adsorption energy, which are only presented here for comparison. As seen from the numerical values of the adsorption energies in Table 1, when an element enters the symmetric structure of the boron nitride nanotube as an impurity, it provides a more active surface for gas adsorption by disturbing the electron cloud. Here the highest adsorption energy occurs when an aluminum atom is placed between the nanotube walls. Also, by adding carbon atoms, a more active surface is provided to adsorb CNCl gas. Therefore, one of the ways to manipulate the nanotubes and optimize adsorption intensity is by doping the element in the outer nanotube wall.

3.2. Electronic properties

Population analysis is used to calculate charge transfer. One of the most popular methods for calculating charge transfer is the NBO method (see next section). The nature of the nanotube total density of states (TDOS) around the Fermi energy level is critical to figure out the electrical transport through this systems. Fig. 5 shows how the electrons are distributed on the energy levels below the HOMO as well as above the LUMO, together with the changes in the energy gap during the adsorption process. Evidently, the largest change in the energy gap is found for the gas/BNAlNT system. For the isolated BNAlNT, the energy gap value is 9.193 eV, while for the gas/BNAlNT system, this decreases to 8.199 eV. This dramatic change in energy gap indicates that BNAlNT is very sensitive to gas adsorption, which can be attributed to the electronic specifications of the system. We should note here that the hybridization of the aluminum atom happens at the sp^3 orbitals, which this is in contrast to the boron atom. Therefore, aluminum can also have a coordination number of 4, thus creating more Lewis acid strength. From Tables 1 and 2, it can be concluded that more negative adsorption energy and higher charge transfer attributes higher reactivity to the nanotube doped with aluminum, thus providing a more suitable system for CNCl adsorption.

Typically, the macroscopic properties probed by sensors is their electrical conductivity, which can be calculated as [56]:

$$\sigma = AT^{3/2}\exp\left(\frac{-E_g}{2kT}\right) \tag{4}$$

Here *A* is a constant (?? electrons/m^3 $K^{3/2}$), *T* the …, *Eg* the …, and *k* the Boltzmann constant. According to Eq. 4, if the energy gap is not very

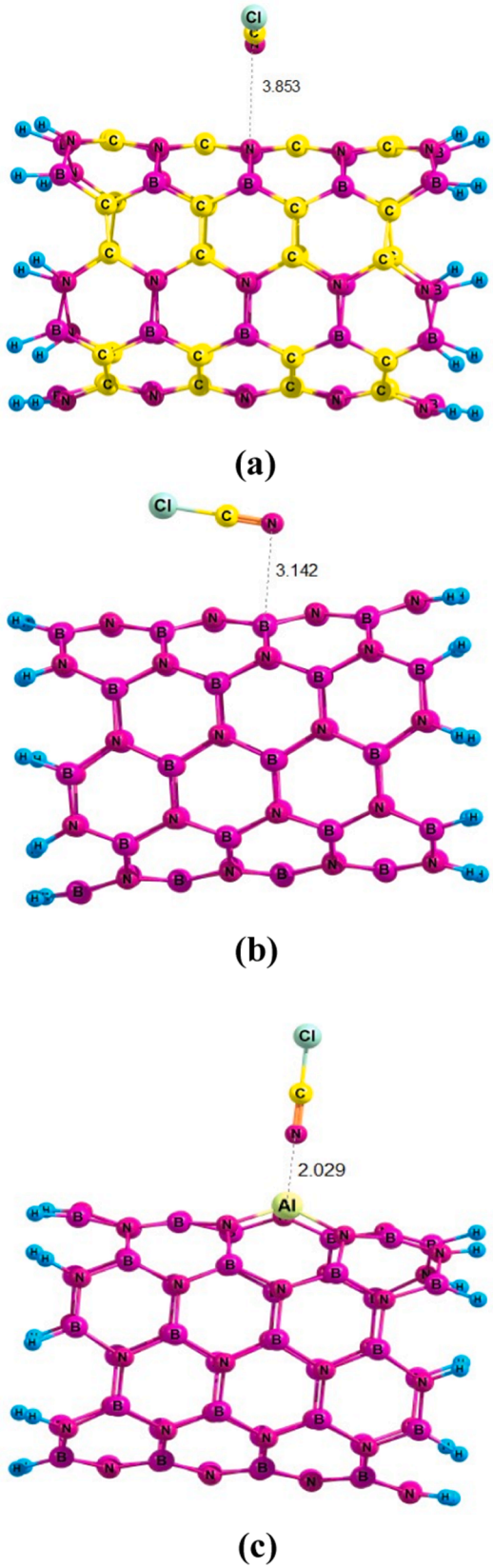

Fig. 4. Structure and equilibrium intermolecular distances of the most stable gas-nanotube states for **(a)** CNCl/BC_2NNT, **(b)** CNCl/BNNT, and **(c)** CNCl/BNAlNT. Calculations are made by the ωB97XD/6-311G(d) model.

Table 1
Calculated adsorption energies (E_{ads}; in eV) for CNCl/BC_2NNT, CNCl/BNNT, and CNCl/BNAlNT using different functionals and the 6-311G(d) basis set.

Systems	B3LYP-D3	M06-2X	ωB97XD
CNCl/BC_2NNT	−0.246	−0.222	−0.281
CNCl/BNNT	−0.236	−0.191	−0.256
CNCl/BNAlNT	−1.143	−1.139	−1.175

large, the electrical conductivity is significant, which can produce the appropriate signal in the relevant circuit. According to the values listed in Table 2, the reported energy gaps are in the desired range, and therefore there is the ability to design sensors from these nanotubes, especially boron nitride nanotube doped with aluminum. To ensure the correctness of the calculations made, the calculations related to the frequency have also been performed. By referring to Table S1 and S2 in supplementary materials, one can correctly check the information related to thermochemistry. Furthermore, it is clear that no negative frequencies are observed, so the geometric optimization information is reported correctly.

3.3. NBO analysis

NBO is employed to further follow up on what happens during the adsorption process. As the gas molecule approaches the surface of the electron cloud nanotube, the two species participating in the interaction merge with each other, and at this point one can calculate the charge transfer rate by NBO analysis. The values shown in Table 2indicate that electrons move between the gas and the nanotube. To assess the intensity of adsorption, another parameter that can be used from the general form of NBO analysis is the bond order, which can be described by various methods. Weiberg bond index [57,58], Meyer [59–61] and Mulliken [62] bond orders are among the most common, which can be calculated from the following relationships:

$$I_{AB} = \sum_i \eta_i \sum_{a\in A}\sum_{b\in B} 2C_{a,i}C_{b,i}S_{a,b} = 2\sum_{a\in A}\sum_{b\in B} P_{a,b}S_{a,b} \quad (5)$$

$$I_{AB} = I^{\alpha}_{AB} + I^{\beta}_{AB} = 2\sum_{a\in A}\sum_{b\in B}\left[(P^{\alpha}S)_{ba}(P^{\alpha}S)_{ab} + \left(P^{\beta}S\right)_{ba}\left(P^{\beta}S\right)_{ab}\right] \quad (6)$$

$$I_{AB} = \sum_{a\in A}\sum_{b\in B} P^2_{ab} \quad (7)$$

Having a density matrix P and an overlap matrix S, the bond order can be easily reported. Equation 5 shows Mulliken bond order and equations 6 and 7 show Mayer order and Wiberg bond index, respectively. Numerical values obtained from the mentioned methods are provided in Table 3. Evidently, the order of bonding between the two species participating in the adsorption process exhibits a maximum value for the nanotubes containing Al.

3.4. Qtaim analysis

To determine the type of intermolecular interactions that may occur during the adsorption process, Bader [63,64] developed the QTAIM comprehensive method of analysis. In this method, by defining a number of parameters (see below), one can determine the type of interaction, whether covalent or non-covalent, and thus determine the type of adsorption process, whether chemical or physical. The electron density $\rho(\mathbf{r})$, which plays a fundamental role in DFT calculations, is employed here as well, and from it, other useful parameters in QTAIM analysis can be obtained. In this analysis, if we derive the electron density and set it to zero ($\nabla\rho(\mathbf{r}) = 0$), we can determine the critical points that represent local maxima or minima. Other parameters that can be used in QTAIM analysis to describe the type of intermolecular interactions are the kinetic electron density $G(\mathbf{r})$, Laplacian of electron density $\nabla^2\rho(\mathbf{r})$, and

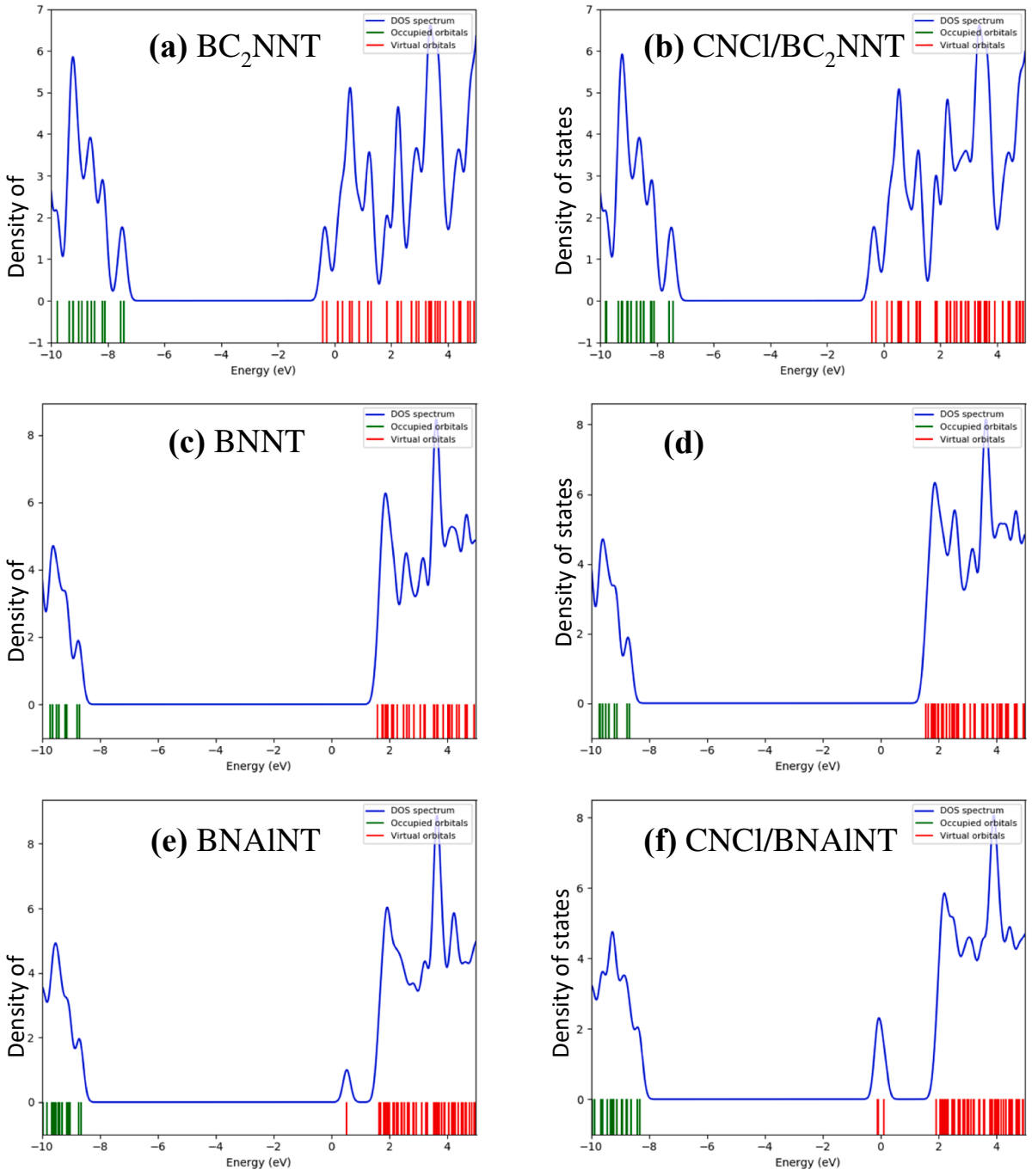

Fig. 5. Density of the states (DOS) for systems: **(a)** BC_2NNT, **(b)** CNCl/BC2NNT, **(c)** BNNT, **(d)** CNCl/BNNT, **(e)** BNAlNT, and **(f)** CNCl/BNAlNT. The implemented model chemistry is ωB97XD/6-311G(d).

Table 2
The HOMO (ε_H) and LUMO (ε_L) energy values; HOMO–LUMO energy gap (E_g). All values are in eV. Q_T denotes the total Mulliken charge for molecules at ωB97XD/6-311G(d) level of theory.

Systems	ε_H	ε_L	E_g	$Q_T(\|e\|)$
BC_2NNT	−7.428	−0.401	7.027	–
BNNT	−8.693	−1.603	7.090	–
BNAlNT	−8.660	0.533	9.193	–
CNCl/BC_2NNT	−7.431	−0.405	7.025	0.039
CNCl/BNNT	−8.675	−1.566	7.109	0.048
CNCl/BNAlNT	−8.309	−0.110	8.199	0.229

Table 3
The Mullike and Mayer bond order values as well as Wiberg bond index (WBI) calculated by ωB97XD/6-311G(d) level of theory through NBO analysis.

Systems	Mulliken	Mayer	Wiberg
CNCl/BC_2NNT	0.025	0.066	0.139
CNCl/BNNT	0.019	0.027	0.101
CNCl/BNAlNT	0.130	0.220	0.343

potential electron density $V(\mathbf{r})$ [65].

Intermolecular interactions are of the covalent type when the amount of electron density $\rho(\mathbf{r})$ is large and its Laplacian is negative

($\nabla^2\rho(\mathbf{r}) < 0$). If the Laplacian is positive and the value of $\rho(\mathbf{r})$ is low, the interactions are of non-covalent type and can be of closed-shell or van der Waals type [66]. Table 4 lists the values of each of these parameters at the critical points depicted in Fig. 6. Here the Laplacian values are positive and the electron density is negligible, so for all the studied systems, the intermolecular interactions are non-covalent.

According to the viral theorem, electron density can be related to the Lagrangian kinetic energy $G(\mathbf{r})$ and the potential energy density $V(\mathbf{r})$, which is represented by the following relationship [67]:

$$\frac{1}{4}\nabla^2\rho(\boldsymbol{r}) = 2G(\boldsymbol{r}) + V(\boldsymbol{r}) \tag{8}$$

The ratio of the last two parameters, $G(\mathbf{r})/|V|(\mathbf{r})$, is so important that if it is<0.5, the intermolecular interactions are covalent. Conversely, if the ratio is between 0.5 and 1, the bond is non-covalent, but if it is greater than 1, intermolecular interactions are considered as van der Waals interactions. The value of this ratio is greater than one for all systems as shown in Table 4, so the type of interaction can be considered van der Waals.Consequently, the intermolecular interactions cannot be in the field of chemical adsorption, but of physical adsorption.

3.5. Nci analysis

The results obtained from the previous sections show that the interactions between the CNCl gas molecule and nanotubes are non-covalent. To verify this, the interactions were examined in terms of non-covalent interaction (NCI) analysis to determine the accuracy of the results. This analysis has been used in many articles to determine the role of van der Waals type intermolecular interactions [68–75]. NCI analysis uses two parameters: (1) $\mathrm{sign}\lambda_2(\mathbf{r})\rho(\mathbf{r})$, which is the product of electron density and the sign of the second Hessian eigenvector, and (2) The Reduced Density Gradient (RDG), which is a dimensionless form of a gradient of electron density [76], given by:

$$RDG(\boldsymbol{r}) = \frac{1}{2(3\pi^2)^{\frac{1}{3}}}\frac{|\nabla\rho(\boldsymbol{r})|}{\rho(\boldsymbol{r})^{\frac{4}{3}}} \tag{8}$$

Here, in the nominator, the absolute value of the electron density gradient is placed, and the variable in the denominator is the electron density. The relation between of these two parameters are shown in Fig. 7. Three areas can be distinguished in Fig. 7, indicating the type of interactions. The $\mathrm{sign}\lambda_2(\mathbf{r})\rho(\mathbf{r}) < 0$ region, is characterised by strong non-covalent interactions (i.e. H-bond and Halogen-bond), the $\mathrm{sign}\lambda_2(\mathbf{r})\rho(\mathbf{r}) \approx 0$ region, by relatively weak van der Waals interactions, and the $\mathrm{sign}\lambda_2(\mathbf{r})\rho(\mathbf{r})$ greater than 0 region, by repulsion forces [76,77]. These areas are marked with blue, green and red colors in Fig. 7, respectively. The strength of weak intermolecular bonds has a direct relationship with the electron density. In the case of van der Waals interactions, the value of the electron density is close to zero. Meanwhile, hydrogen and halogen bonds have a large electron density value.

Repetitive results from previous analyses are also shown in the NCI analysis through. When the electron density and the second eigenvector of the Hessian matrix are both close to zero ($\lambda_2(\mathbf{r}) \approx 0$, $\rho(\mathbf{r}) \approx 0$), the accumulation of points at this region in the two-dimensional diagram indicates the presence of van der Waals type interactions. When we look at the two-dimensional diagrams for the isolated absorbers (Fig. 7 (a), (c), and (e)), there are no points in the mentioned region. Meanwhile, when the gas molecule is placed on the absorbers (Fig. 7 (b), (d), and (e)), points appear in this area, which indicates the existence of intermolecular interactions of the van der Waals type.

Table 4
Parameters extracted from QTAIM calculations: electron density ($\rho(\mathbf{r})$) and ($\nabla^2\rho(\mathbf{r})$) shows Laplacian of electron density. The kinetic electron density $G(\mathrm{r})$ and potential electron density $V(\mathbf{r})$, and their ratio $G(\mathbf{r})/V(\mathbf{r})$ at BCPs are also listed. The implemented model chemistry ωB97XD/6-311G(d).

Systems	ρ(r)	$\nabla^{2\rho}$(r)	G(r)	V(r)	G(r)/V(r)
CNCl/BC_2NNT	0.0068	0.0203	0.0042	−0.0033	1.2758
CNCl/BNNT	0.0060	0.0191	0.0039	−0.0031	1.2648
CNCl/BNAlNT	0.0448	0.2764	0.0655	−0.0619	1.0585

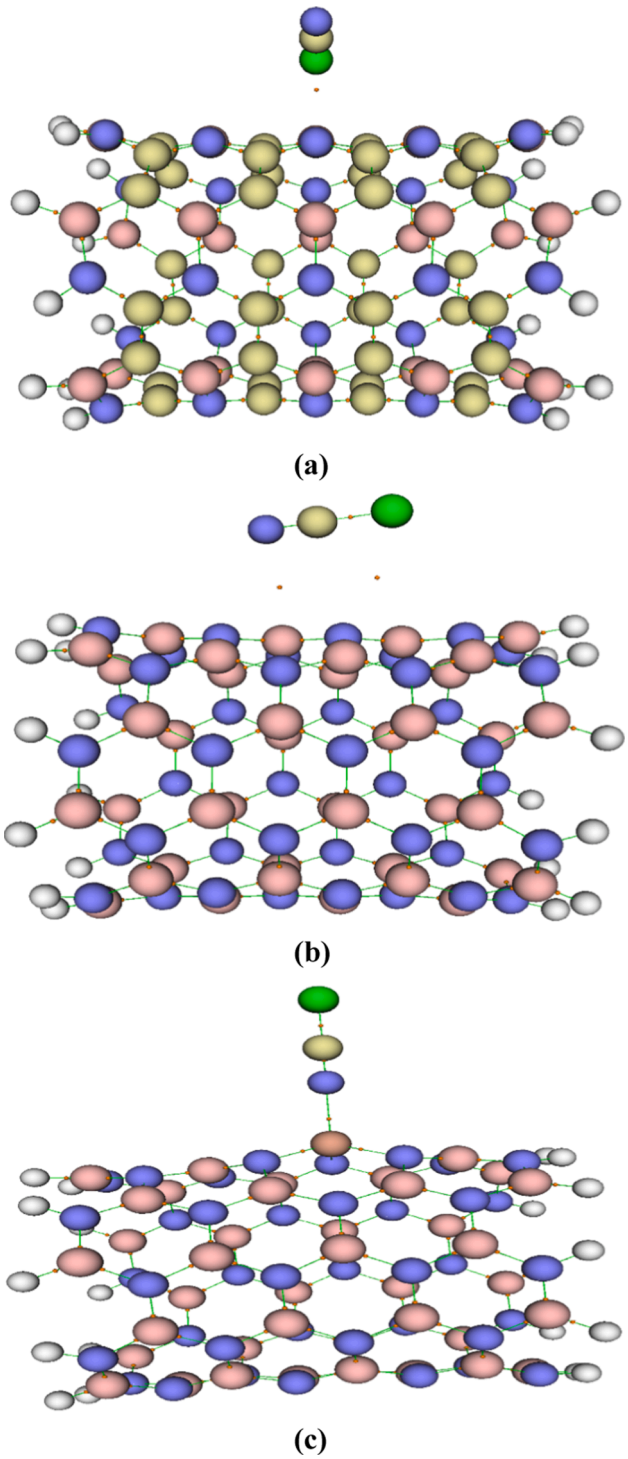

Fig. 6. Graphs related to atom in molecules analysis (QTAIM). Orange dots represent the boundary critical points (BCPs). The molecules are displayed as follows: **(a)** CNCl/BC_2NNT, **(b)** CNCl/BNNT, and **(c)** CNCl/BNAlNT systems. The implemented model chemistry ωB97XD/6-311G(d). (For interpretation of the references to color in this figure legend, the reader is referred to the web version of this article.)

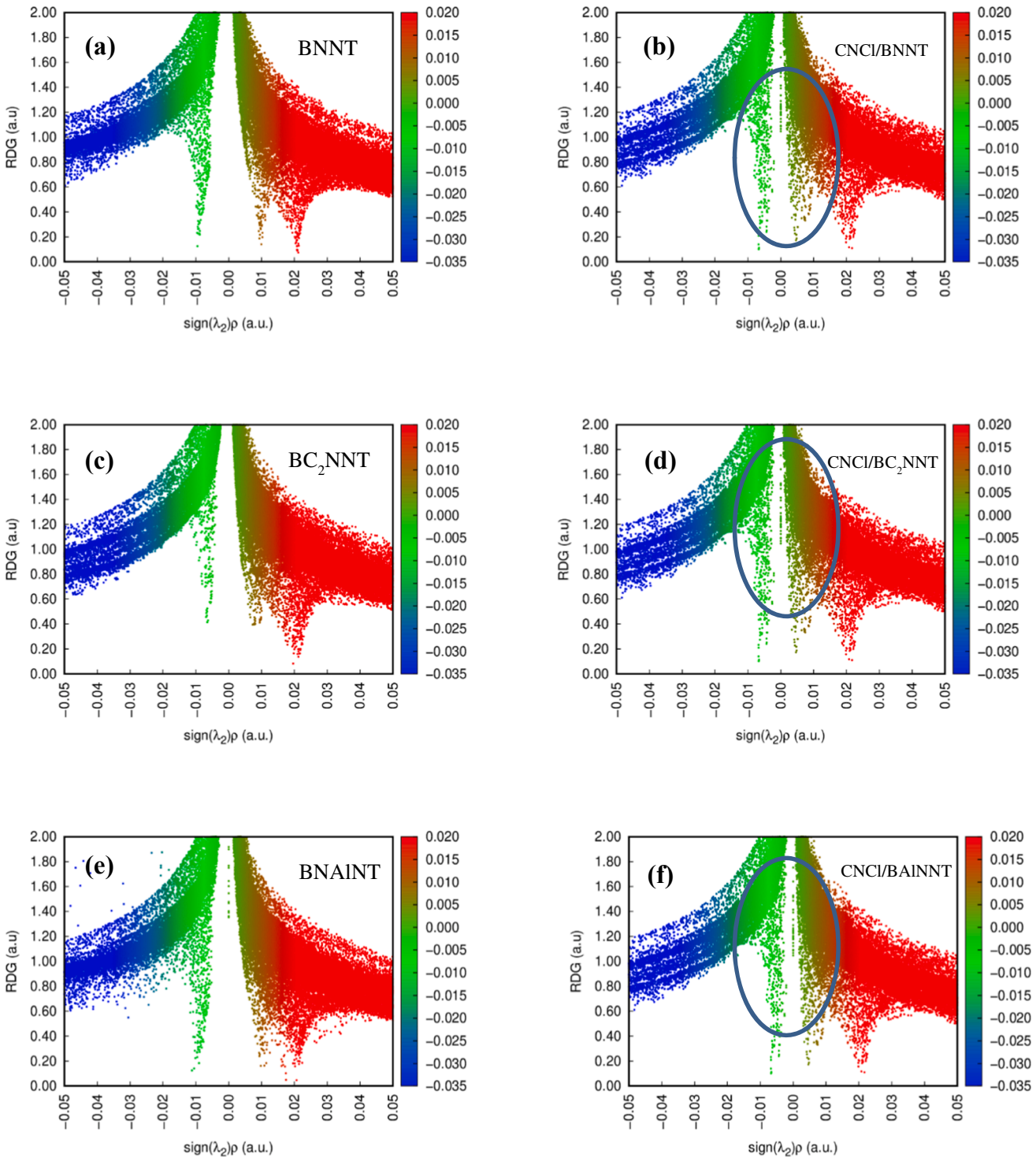

Fig. 7. Reduced density gradient (RDG) vs sign(λ_2)ρ(r) values for **(a)** BC_2NNT, **(b)** CNCl/BC2NNT, **(c)** BNNT, **(d)** CNCl/BNNT, **(e)** BNAlNT, and **(f)** CNCl/BNAlNT. The data were obtained from B3LYP-D3/6-311G(d) level of theory. The left side diagrams refer to isolated nanotubes and the right side diagrams are CNCl/ nanotubes. The three areas marked in blue, green and red color are related to strong attraction interactions, van der Waals interactions and strong repulsion interactions, respectively. (For interpretation of the references to color in this figure legend, the reader is referred to the web version of this article.)

4. Conclusion

The intermolecular interactions between pollutant and lethal cyanogen chloride gas with BNNT, BNAlNT, and BC_2NNT was investigated. All calculations are performed at the DFT level of study. The chemistry model used in the wave function analysis calculations was B3LYP-D3 (GD3BJ)/6-311G(d). The ωB97XD as well as M06-2X functionals have also been used for the geometry optimization.

The calculations show that adsorption of CNCl by these nanotubes is possible. During the adsorption process, the energy gap changes significantly, which is desirable for designing and building sensors. Among the investigated nanotubes, BNAlNT has the highest adsorption energy and the strongest intermolecular interaction with the target gas, and therefore it is recommended for CNCl sensors. Charge transfer analysis

by the NBO method show that this happens from the nitrogen atom of the gas molecule to the nanotubes. The parameters obtained by the QTAIM analysis indicate that the interaction between the molecules is non-covalent and the adsorption process can be classified as physical.

CRediT authorship contribution statement

Mohsen Doust Mohammadi: Writing – original draft, Formal analysis. **Hewa Y. Abdullah:** Supervision, Investigation, Project administration. **George Biskos:** Conceptualization, Validation. **Somnath Bhowmick:** Resources, Visualization.

Declaration of Competing Interest

The authors declare that they have no known competing financial interests or personal relationships that could have appeared to influence the work reported in this paper.

Data availability

No data was used for the research described in the article.

Acknowledgments

HYA thanks the Solid-State Theory Group, Physics Department, Università degli Studi di Milano, Milan, Italy, for providing computational facilities. SB and GB acknowledge the support of the European Regional Development Fund and the Republic of Cyprus through the Research Innovation Foundation (Cy-Tera project under the grant NEA YPODOMH/STPATH/0308/31, and NANO2LAB project under the grant INFRASTRUCTURES/1216/0070).

Appendix A. Supplementary material

Supplementary data to this article can be found online at https://doi.org/10.1016/j.comptc.2022.113980.

References

[1] C.P. Poole Jr, F.J. Owens, Introduction to nanotechnology, John Wiley & Sons, 2003.
[2] M.S. Islam, T. Hussain, G. Rao, P. Panigrahi, R. Ahuja, Augmenting the sensing aptitude of hydrogenated graphene by crafting with defects and dopants, Sens. Actuators B 228 (2016) 317–321.
[3] T. Hussain, M. Hankel, D.J. Searles, Improving sensing of sulfur-containing gas molecules with ZnO monolayers by implanting dopants and defects, J. Phys. Chem. C 121 (2017) 24365–24375.
[4] S. Deshpande, M. Deshpande, T. Hussain, R. Ahuja, Binding and optical characteristics of polycyclic aromatic hydrocarbons and their nitroderivatives adsorbed on the C 3 N monolayer, New J. Chem. 46 (2022) 2245–2258.
[5] M.D. Mohammadi, M. Hamzehloo, The adsorption of bromomethane onto the exterior surface of aluminum nitride, boron nitride, carbon, and silicon carbide nanotubes: a PBC-DFT, NBO, and QTAIM study, Comput. Theor. Chem. 1144 (2018) 26–37.
[6] H. Sun, Ab initio calculations and force field development for computer simulation of polysilanes, Macromolecules 28 (1995) 701–712.
[7] R.A. Kendall, H.A. Früchtl, The impact of the resolution of the identity approximate integral method on modern ab initio algorithm development, Theor. Chem. Acc. 97 (1997) 158–163.
[8] M.D. Mohammadi, H.Y. Abdullah, DFT Study for Adsorbing of Bromine Monochloride onto BNNT (5, 5), BNNT (7, 0), BC 2 NNT (5, 5), and BC 2 NNT (7, 0), Journal of Computational Biophysics and Chemistry 20 (2021) 765–783.
[9] M.D. Mohammadi, H.Y. Abdullah, S. Bhowmick, G. Biskos, Theoretical investigation of X12O12 (X= Be, Mg, and Ca) in sensing CH2N2: A DFT study, Comput. Theor. Chem. 1198 (2021), 113168.
[10] M.D. Mohammadi, H.Y. Abdullah, S. Bhowmick, G. Biskos, A comprehensive investigation of the intermolecular interactions between CH2N2 and X12Y12 (X= B, Al, Ga; Y= N, P, As) nanocages, Can. J. Chem. 99 (2021) 733–741.
[11] M.D. Mohammadi, H.Y. Abdullah, G. Biskos, S. Bhowmick, Enhancing the absorption of 1-chloro-1, 2, 2, 2-tetrafluoroethane on carbon nanotubes: an ab initio study, Bull. Mater. Sci. 44 (2021) 198.
[12] M.D. Mohammadi, H.Y. Abdullah, G. Biskos, S. Bhowmick, Effect of Al-and Ga-doping on the adsorption of H2SiCl2 onto the outer surface of boron nitride nanotube: a DFT study, C. R. Chim. 24 (2021) 291–304.
[13] M.D. Mohammadi, H.Y. Abdullah, V. Kalamse, A. Chaudhari, Adsorption of alkali and alkaline earth ions on nanocages using density functional theory, Comput. Theor. Chem. 1204 (2021), 113391.
[14] M.D. Mohammadi, H.Y. Abdullah, A. Suvitha, The adsorption of 1-chloro-1, 2, 2, 2-Tetrafluoroethane onto the pristine, Al-, and Ga-doped boron nitride nanosheet, Iranian Journal of Science and Technology, Transactions A, Science 45 (2021) 1287–1300.
[15] P.G. Collins, A. Zettl, H. Bando, A. Thess, R. Smalley, Nanotube nanodevice, Science 278 (1997) 100–102.
[16] C. Ewels, M. Glerup, Nitrogen doping in carbon nanotubes, J. Nanosci. Nanotechnol. 5 (2005) 1345–1363.
[17] P. Ayala, R. Arenal, M. Rümmeli, A. Rubio, T. Pichler, The doping of carbon nanotubes with nitrogen and their potential applications, Carbon 48 (2010) 575–586.
[18] P. Shao, X.-Y. Kuang, L.-P. Ding, J. Yang, M.-M. Zhong, Can CO2 molecule adsorb effectively on Al-doped boron nitride single walled nanotube? Appl. Surf. Sci. 285 (2013) 350–356.
[19] M. Mirzaei, A. Nouri, The Al-doped BN nanotubes: a DFT study, J. Mol. Struct. (Thoechem) 942 (2010) 83–87.
[20] M. Doust Mohammadi, H.Y. Abdullah, Adsorption of 1-chloro-1, 2, 2, 2-tetrafluoroethane on pristine, Al, Ga-doped boron nitride nanotubes: a study involving PBC-DFT, NBO analysis, and QTAIM, Can. J. Chem. 99 (2021) 51–62.
[21] S. Peng, K. Cho, Ab initio study of doped carbon nanotube sensors, Nano Lett. 3 (2003) 513–517.
[22] M. Eising, C.E. Cava, R.V. Salvatierra, A.J.G. Zarbin, L.S. Roman, Doping effect on self-assembled films of polyaniline and carbon nanotube applied as ammonia gas sensor, Sens. Actuators B 245 (2017) 25–33.
[23] L. Zhao, M. Choi, H.-S. Kim, S.-H. Hong, The effect of multiwalled carbon nanotube doping on the CO gas sensitivity of SnO2-based nanomaterials, Nanotechnology 18 (2007), 445501.
[24] A. Watson, L. Hall, E. Raber, V.D. Hauschild, F. Dolislager, A.H. Love, M.L. Hanna, Developing health-based pre-planning clearance goals for airport remediation following chemical terrorist attack: Introduction and key assessment considerations, Hum. Ecol. Risk Assess. 17 (2011) 2–56.
[25] B.A. Farooqi, M. Yar, A. Ashraf, U. Farooq, K. Ayub, Graphene-polyaniline composite as superior electrochemical sensor for detection of cyano explosives, Eur. Polym. J. 138 (2020), 109981.
[26] N. Isaac, I. Pikaar, G. Biskos, Metal oxide semiconducting nanomaterials for air quality gas sensors: operating principles, performance, and synthesis techniques, Microchim. Acta 189 (2022) 1–22.
[27] M. Rouhani, DFT study on adsorbing and detecting possibility of cyanogen chloride by pristine, B, Al, Ga, Si and Ge doped graphene, J. Mol. Struct. 1181 (2019) 518–535.
[28] S.V. Sawant, A.W. Patwardhan, J.B. Joshi, K. Dasgupta, Boron doped carbon nanotubes: Synthesis, characterization and emerging applications–A review, Chem. Eng. J. 427 (2022), 131616.
[29] M.T. Baei, M.R. Taghartapeh, A. Soltani, K.H. Amirabadi, N. Gholami, Interaction of pure and metal atom substituted carbon nanocages with CNCl: a DFT study, Russian, J. Phys. Chem. B 11 (2017) 354–360.
[30] A. Soltani, A. Sousaraei, M. Mirarab, H. Balakheyli, Interaction of CNCl molecule and single-walled AlN nanotubes using DFT and TD-DFT calculations, J. Saudi Chem. Soc. 21 (2017) 270–276.
[31] M. Ghadiri, M. Ghambarian, M. Ghashghaee, Detection of CNX cyanogen halides (X= F, Cl) on metal-free defective phosphorene sensor: periodic DFT calculations, Mol. Phys. 119 (2021) e1819577.
[32] P. Snehha, V. Nagarajan, R. Chandiramouli, Interaction behavior of cyanogen fluoride and chloride gas molecules on red phosphorene nanosheet: a DFT study, J. Inorg. Organomet. Polym Mater. 29 (2019) 954–963.
[33] L. Goerigk, S. Grimme, A thorough benchmark of density functional methods for general main group thermochemistry, kinetics, and noncovalent interactions, PCCP 13 (2011) 6670–6688.
[34] N. Mardirossian, M. Head-Gordon, Thirty years of density functional theory in computational chemistry: an overview and extensive assessment of 200 density functionals, Mol. Phys. 115 (2017) 2315–2372.
[35] A. Brakestad, S.R. Jensen, P. Wind, M. D'Alessandro, L. Genovese, K.H. Hopmann, L. Frediani, Static polarizabilities at the basis set limit: A benchmark of 124 species, J. Chem. Theory Comput. 16 (2020) 4874–4882.
[36] H. Mitra, T.K. Roy, Comprehensive Benchmark Results for the Accuracy of Basis Sets for Anharmonic Molecular Vibrations, Chem. A Eur. J. 124 (2020) 9203–9221.
[37] L. Goerigk, A. Hansen, C. Bauer, S. Ehrlich, A. Najibi, S. Grimme, A look at the density functional theory zoo with the advanced GMTKN55 database for general main group thermochemistry, kinetics and noncovalent interactions, PCCP 19 (2017) 32184–32215.
[38] J.-D. Chai, M. Head-Gordon, Long-range corrected hybrid density functionals with damped atom–atom dispersion corrections, PCCP 10 (2008) 6615–6620.
[39] Y. Zhao, D.G. Truhlar, The M06 suite of density functionals for main group thermochemistry, thermochemical kinetics, noncovalent interactions, excited states, and transition elements: two new functionals and systematic testing of four M06-class functionals and 12 other functionals, Theor. Chem. Acc. 120 (2008) 215–241.
[40] Y. Zhao, D.G. Truhlar, Density functional for spectroscopy: no long-range self-interaction error, good performance for Rydberg and charge-transfer states, and better performance on average than B3LYP for ground states, Chem. A Eur. J. 110 (2006) 13126–13130.
[41] S. Grimme, Semiempirical GGA-type density functional constructed with a long-range dispersion correction, J. Comput. Chem. 27 (2006) 1787–1799.

[42] S. Grimme, J. Antony, S. Ehrlich, H. Krieg, A consistent and accurate ab initio parametrization of density functional dispersion correction (DFT-D) for the 94 elements H-Pu, J. Chem. Phys. 132 (2010), 154104.
[43] S. Grimme, S. Ehrlich, L. Goerigk, Effect of the damping function in dispersion corrected density functional theory, J. Comput. Chem. 32 (2011) 1456–1465.
[44] M.J. Frisch, G.W. Trucks, H.B. Schlegel, G.E. Scuseria, M.A. Robb, J.R. Cheeseman, G. Scalmani, V. Barone, G.A. Petersson, H. Nakatsuji, X. Li, M. Caricato, A.V. Marenich, J. Bloino, B.G. Janesko, R. Gomperts, B. Mennucci, H.P. Hratchian, J.V. Ortiz, A.F. Izmaylov, J.L. Sonnenberg, Williams, F. Ding, F. Lipparini, F. Egidi, J. Goings, B. Peng, A. Petrone, T. Henderson, D. Ranasinghe, V.G. Zakrzewski, J. Gao, N. Rega, G. Zheng, W. Liang, M. Hada, M. Ehara, K. Toyota, R. Fukuda, J. Hasegawa, M. Ishida, T. Nakajima, Y. Honda, O. Kitao, H. Nakai, T. Vreven, K. Throssell, J.A. Montgomery Jr., J.E. Peralta, F. Ogliaro, M.J. Bearpark, J.J. Heyd, E.N. Brothers, K.N. Kudin, V.N. Staroverov, T.A. Keith, R. Kobayashi, J. Normand, K. Raghavachari, A.P. Rendell, J.C. Burant, S.S. Iyengar, J. Tomasi, M. Cossi, J.M. Millam, M. Klene, C. Adamo, R. Cammi, J.W. Ochterski, R.L. Martin, K. Morokuma, O. Farkas, J.B. Foresman, D.J. Fox, Gaussian 16 Rev. C.01, Wallingford, CT, 2016.
[45] R. Dennington, T.A. Keith, J.M. Millam, GaussView, version 6.0. 16, Semichem Inc. Shawnee Mission KS, (2016).
[46] a.J. Foster, F. Weinhold, Natural hybrid orbitals, Journal of the American Chemical Society, 102 (1980) 7211-7218.
[47] A.E. Reed, F. Weinhold, Natural bond orbital analysis of near-Hartree–Fock water dimer, J. Chem. Phys. 78 (1983) 4066–4073.
[48] J. Carpenter, F. Weinhold, Analysis of the geometry of the hydroxymethyl radical by the "different hybrids for different spins" natural bond orbital procedure, J. Mol. Struct. (Thoechem) 169 (1988) 41–62.
[49] T. Lu, F. Chen, Multiwfn: a multifunctional wavefunction analyzer, J. Comput. Chem. 33 (2012) 580–592.
[50] M. Doust Mohammadi, H.Y. Abdullah, Non-covalent interactions of Cysteine onto C60, C59Si, and C59Ge: A DFT study, J. Mol. Model. 27 (2021) 330.
[51] M. Doust Mohammadi, H.Y. Abdullah, Intermolecular interactions between serine and C60, C59Si, and C59Ge: a DFT Study, Silicon, 14(2021) 6075–6088.
[52] M.D. Mohammadi, H.Y. Abdullah, Vinyl chloride adsorption onto the surface of pristine, Al-, and Ga-doped boron nitride nanotube: A DFT study, Solid State Commun. 337 (2021), 114440.
[53] D. Farmanzadeh, S. Ghazanfary, DFT studies of functionalized zigzag and armchair boron nitride nanotubes as nanovectors for drug delivery of collagen amino acids, Struct. Chem. 25 (2014) 293–300.
[54] H. Sargazi-Avval, M. Yoosefian, M. Ghaffari-Moghaddam, M. Khajeh, M. Bohlooli, Potential applications of armchair, zigzag, and chiral boron nitride nanotubes as a drug delivery system: Letrozole anticancer drug encapsulation, Appl. Phys. A 127 (2021) 1–7.
[55] D. Farmanzadeh, S. Ghazanfary, Interaction of vitamins A, B1, C, B3 and D with zigzag and armchair boron nitride nanotubes: a DFT study, C. R. Chim. 17 (2014) 985–993.
[56] S.S. Li, Energy Band Theory (2006) 61–104.
[57] K.B. Wiberg, Application of the pople-santry-segal CNDO method to the cyclopropylcarbinyl and cyclobutyl cation and to bicyclobutane, Tetrahedron 24 (1968) 1083–1096.
[58] O.V. Sizova, L.V. Skripnikov, A.Y. Sokolov, Symmetry decomposition of quantum chemical bond orders, J. Mol. Struct. (Thoechem) 870 (2008) 1–9.
[59] I. Mayer, Charge, bond order and valence in the AB initio SCF theory, Chem. Phys. Lett. 97 (1983) 270–274.
[60] I. Mayer, Improved definition of bond orders for correlated wave functions, Chem. Phys. Lett. 544 (2012) 83–86.
[61] A.J. Bridgeman, G. Cavigliasso, L.R. Ireland, J. Rothery, The Mayer bond order as a tool in inorganic chemistry, J. Chem. Soc. Dalton Trans. (2001) 2095–2108.
[62] R.S. Mulliken, Electronic population analysis on LCAO–MO molecular wave functions, I, The Journal of Chemical Physics 23 (1955) 1833–1840.
[63] R.F. Bader, Atoms in molecules, Acc. Chem. Res. 18 (1985) 9–15.
[64] R. Bader, A Quantum Theory, Clarendon, Oxford, 1990.
[65] R.F.W. Bader, P.L.A. Popelier, T.A. Keith, Theoretical definition of a functional group and the molecular orbital paradigm, Angew. Chem. Int. Ed. Eng. 33 (1994) 620–631.
[66] C.F. Matta, Hydrogen-Hydrogen Bonding: The Non-Electrostatic Limit of Closed-Shell Interaction Between Two Hydro, Hydrogen Bonding—New Insights, Springer, 2006, pp. 337–375.
[67] S.J. Grabowski, QTAIM characteristics of halogen bond and related interactions, Chem. A Eur. J. 116 (2012) 1838–1845.
[68] M. Doust Mohammadi, H.Y. Abdullah, Ab initio investigation for the adsorption of acrolein onto the surface of C60, C59Si, and C59Ge: NBO, QTAIM, and NCI analyses, Structural Chemistry, 33 (2022) 363-378.
[69] M. Doust Mohammadi, H.Y. Abdullah, Weak intermolecular interactions of cysteine on BNNT, BNAlNT and BC2NNT: a DFT investigation, Bull. Mater. Sci. 45 (2022) 1–14.
[70] M. Doust Mohammadi, H.Y. Abdullah, Interaction of the Serine Amino Acid with BNNT, BNAlNT, and BC2NNT, Arab. J. Sci. Eng. (2022) 1–15.
[71] M. Doust Mohammadi, H.Y. Abdullah, S. Bhowmick, G. Biskos, Silicon Carbide Based Nanotubes as a Sensing Material for Gaseous H2SiCl2, Silicon, (2022) 1-10.
[72] M.D. Mohammadi, F. Abbas, H. Louis, G.E. Mathias, T.O. Unimuke, Trapping of CO, CO2, H2S, NH3, NO, NO2, and SO2 by Polyoxometalate compound, Comput. Theor. Chem. 1215 (2022), 113826.
[73] M.D. Mohammadi, H.Y. Abdullah, V. Kalamse, A. Chaudhari, Interaction of Fluorouracil drug with boron nitride nanotube, Al doped boron nitride nanotube and BC2N nanotube, Comput. Theor. Chem. 1212 (2022), 113699.
[74] M.D. Mohammadi, H.Y. Abdullah, V.G. Kalamse, A. Chaudhari, Interaction of halomethane CH3Z (Z= F, Cl, Br) with X12Y12 (X= B, Al, Ga & Y= N, P, As) nanocages, Comput. Theor. Chem. 1208 (2022), 113544.
[75] M.D. Mohammadi, H.Y. Abdullah, H. Louis, G.E. Mathias, 2D Boron Nitride Material as a sensor for H_2SiCl_2, Comput. Theor. Chem. 1213 (2022), 113742.
[76] E.R. Johnson, S. Keinan, P. Mori-Sánchez, J. Contreras-García, A.J. Cohen, W. Yang, Revealing noncovalent interactions, J. Am. Chem. Soc. 132 (2010) 6498–6506.
[77] J. Contreras-García, E.R. Johnson, S. Keinan, R. Chaudret, J.-P. Piquemal, D. N. Beratan, W. Yang, NCIPLOT: a program for plotting noncovalent interaction regions, J. Chem. Theory Comput. 7 (2011) 625–632.